

# Thermal conductance of InAs nanowire composites

*Ann I. Persson<sup>1+</sup>, Yee Kan Koh<sup>2\*+</sup>, David G. Cahill<sup>2</sup>, Lars Samuelson<sup>3</sup>, and Heiner Linke<sup>1,3</sup>*

<sup>1</sup>Physics Department and Materials Science Institute, University of Oregon, Eugene, OR 97403, USA

<sup>2</sup>Department of Material Science and Engineering, University of Illinois, Urbana, IL 61801, USA

<sup>3</sup>Solid State Physics and The Nanometer Structure Consortium, Lund University, Box 118, 221 00

Lund, Sweden

<sup>+</sup> These authors contributed equally to the work.

ykoh@mrl.uiuc.edu

**RECEIVED DATE (to be automatically inserted after your manuscript is accepted if required according to the journal that you are submitting your paper to)**

Corresponding author: Address: Frederick Seitz Materials Research Lab, 104 South Goodwin Ave, Urbana, IL 61801; Tel: +1 217 244 2207; Fax: +1 217 244 2946; Email: ykoh@mrl.uiuc.edu

The ability to measure and understand heat flow in nanowire-composites is crucial for applications ranging from high-speed electronics to thermoelectrics. Here we demonstrate the measurement of the thermal conductance of nanowire-composites consisting of regular arrays of InAs nanowires embedded in PMMA using time-domain thermoreflectance (TDTR). Based on a proposed model for heat flow in the composite, we can, as a consistency check, extract the thermal conductivity  $\Lambda$  of the InAs nanowires and find  $\Lambda_{NW}=5.3\pm 1.5 \text{ W m}^{-1} \text{ K}^{-1}$ , in good agreement with theory and previous measurements of individual nanowires.

Understanding and controlling heat flow in nanowires (NWs) is important for optimizing heat dissipation in electronic and optoelectronic devices, as well as for minimizing parasitic heat flow in NW-based thermoelectric devices.<sup>1</sup> Scattering of phonons at the surfaces of the NW reduces the lattice thermal conductivity of the NW compared to its bulk counterpart.<sup>2,3</sup>

Most measurements of the thermal conductivity of NWs to date have been carried out on individual NWs, which is an advantage when studying how the thermal conductance is related to the crystal structure and its quality, surface roughness, and diameter of the individual NW.<sup>4-8</sup> However, many future NW-based devices will be based on a large number of densely-packed NWs, perhaps supported by a matrix material, and it may not be the properties of isolated NWs that control the final performance, but rather a combination of the NWs and the matrix material. The resulting thermal conductivity of the NWs and the matrix, the so-called NW-composite, depends on the NW diameter and array geometry,<sup>9,10</sup> but also on the character of the NW/matrix interface and the presence of additional components such as insulating shells and metal wrap-gates in structures for high-speed electronics.<sup>11-13</sup>

Here we demonstrate how to measure the thermal conductance of NW-composites using time-domain thermoreflectance (TDTR), a technique that has previously been established for characterization of the thermal transport properties of thin films and interfaces.<sup>14,15</sup> Our measurements show that the thermal conductivity of the NW-composite as measured by TDTR depends on the penetration depth of the thermal waves that are used in the experiment. We relate this behavior to the length-scale for temperature equilibration between the NWs and the surrounding matrix material by carrying out finite element method (FEM) analysis of the heat flow through the NW-composite. This procedure also allows us to determine the thermal conductivity of the NWs in the NW-composite.

For this first test of the use of TDTR for measurements of NW-arrays, the following conditions are important for the NW-samples. First, to ensure sufficient sensitivity to the properties of the NWs, the areal packing density should be high. Second, a thin Al film is required on top of the NWs to provide a surface with high thermoreflectance for TDTR measurements. Third, to facilitate data interpretation, the top ends of the NWs should be in contact with the thin Al film without roughening the surface of the Al

too much and affecting the optical properties of the Al film. Therefore, NWs of uniform length are desired.

The NWs were nucleated by Au seed particles deposited on an InAs (111)B substrate and grown using chemical beam epitaxy (CBE). For growth of NW arrays with high areal packing density in this growth system, where the NWs start competing for growth material if they are spaced less than  $\sim 1 \mu\text{m}$ , the growth rate and final length depend on both the spacing and the diameter of the NWs.<sup>16,17</sup> Therefore, to achieve a uniform length of the NWs it is necessary to ensure that the NWs are evenly spaced and have the same diameter. For seed particles, we used Au discs fabricated by electron-beam lithography, thermal evaporation and lift-off.<sup>17</sup> The Au discs were positioned in a hexagonal lattice, such that each disc in the  $90 \times 90 \mu\text{m}^2$  array was separated from its six nearest neighbors with a spacing of 200 nm. Trimethylindium and tertiarybutylarsine were used as group-III and group-V growth sources with source pressures 0.15 mbar and 1.5 mbar respectively and the growth temperature was  $\approx 430^\circ\text{C}$ . Figure 1 shows images taken with a scanning electron microscope (SEM) of the NW array after growth. The resulting NWs were  $52 \pm 4 \text{ nm}$  in diameter, and had an areal packing density of  $x=0.061 \pm 0.009$ . The lengths of the NWs were  $430 \pm 40 \text{ nm}$ , which corresponds to a growth rate of 8.6 nm/min. This growth rate is in good agreement with previous results of growth of NWs of the same diameter and spacing.<sup>17</sup>

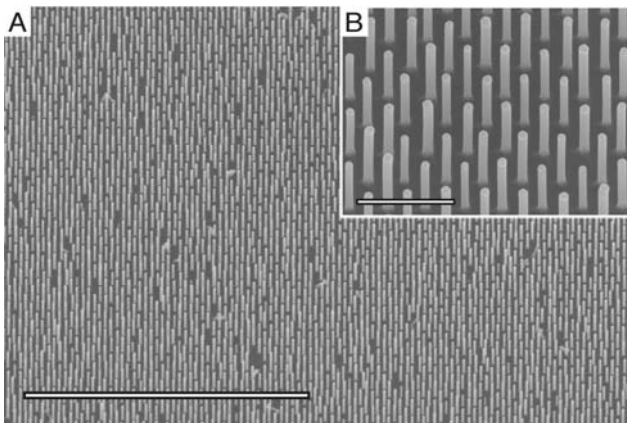


**Figure 1.** (A) SEM image of the InAs NW array grown perpendicular on a (111) B InAs substrate. For imaging, the NWs were tilted  $30^\circ$ . The scale bar is  $5 \mu\text{m}$ . (B) SEM image of the same array as in A, but larger magnification. The scale bar is  $500 \text{ nm}$ . The NWs are  $52 \pm 4 \text{ nm}$  in diameter and  $430 \pm 40 \text{ nm}$  in

length. The spacing between each NW in the array is 200 nm and the areal packing density  $x = 0.061 \pm 0.009$ .

To deposit the Al layer needed for the TDTR technique, we used the following procedure. After growth, the NW-array was completely embedded in  $\approx 850$  nm thick polymethyl methacrylate (PMMA). Using an ozone plasma, the PMMA layer was then etched down until the tops of the NWs in the array were above the PMMA surface, enough to ensure contact with the Al film without creating excessive unevenness of the Al surface. Finally, a 90 nm thick Al film was deposited by thermal evaporation. Figure 2 shows a schematic of the cross-section of the sample structure and a corresponding SEM image. The PMMA-embedded NW-array will from now on be referred to as the NW-composite. We occasionally observe voids in the NW-composite in some of the SEM images, see Fig. 2c. We estimate the volume percentage of the voids to be  $<2\%$ ; this small volume fraction of voids does not significantly affect our measurements.

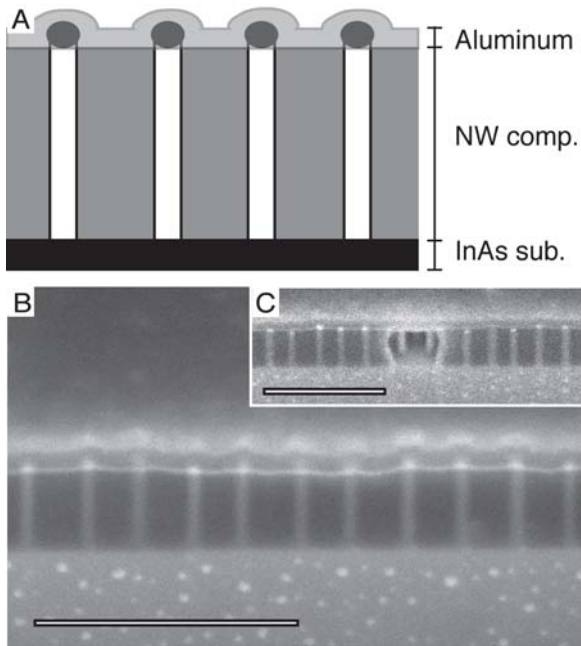


**Figure 2.** (A) Schematic image of the sample structure. The NWs are epitaxially nucleated and grown from an InAs (111) B substrate. The NW-array is then embedded in PMMA, which is etched back until the tops of the NWs are visible above the PMMA surface. Finally, an Al film with high thermoreflectance is deposited on top of the sample. (B) SEM images taken with a  $52^\circ$  tilt of the cross

section of the sample. The cross section became accessible after milling using a focused ion beam, FIB. The scale bar is 1  $\mu\text{m}$ . (C) SEM image showing a void in the NW-composite, which we believe could be due to incomplete PMMA coverage during the spin-on process. We estimate that these voids represent about 2% or less of the total NW-composite volume. The scale bar in the inserted image is also 1  $\mu\text{m}$ .

We measure thermal conductivity  $\Lambda$  by TDTR.<sup>18,19</sup> In TDTR measurements, laser pulses of duration  $<0.3$  ps produced by a Ti:Sapphire laser oscillator at a repetition rate of 80 MHz are split into a pump beam and a probe beam. The  $1/e^2$  radii of the pump and probe beam at the sample surface are  $\approx 7.5$   $\mu\text{m}$ , and the total laser powers are  $\approx 4$  mW, creating steady-state temperature rises of  $<6$  K. The pump beam, modulated at a frequency  $f$  in the range  $0.6 < f < 10$  MHz, heats the sample; each pulse in the pump beam creates an abrupt, instantaneous temperature rise at the surface of the sample. As heat dissipates into the sample, the probe beam is used to monitor the in-phase and out-of-phase temperature oscillation at the surface of the Al film as a function of the relative delay time between pump and probe pulses. The probe beam measures the evolution of the surface temperature through the thermoreflectance  $dR/dT$  — i.e., the change of the reflectivity  $R$  with temperature  $T$  — of the Al film. We use a photodiode and an rf lock-in amplifier to extract the small changes in the reflected intensity of the probe beam. Since the surface morphology of the NW-composite sample shows significant roughness despite the nearly equal heights of the NWs, we employ a newly developed two-tint approach<sup>20</sup> to reject diffusively scattered light from the pump beam.

We analyze the TDTR data by comparing measurements of the ratio of the in-phase and out-of-phase signals of the lock-in amplifier,  $V_{in}(t)/V_{out}(t)$ , to calculations based on the numerical solution of an analytical description of the heat flow in layered structures.<sup>21</sup> In the calculations, we take into account changes of the radius of the pump beam at different delay time.<sup>22</sup> We treat the NW-composite as a homogeneous layer with an average thermal conductivity  $\Lambda_C$ , and estimate the heat capacity  $C_C$  of the layer from the areal-density-weighted average of heat capacity of bulk InAs<sup>23</sup> and PMMA.<sup>24</sup> We approximate the thermal conductivity of the Al film  $\Lambda_{Al}$ , using the Wiedemann-Franz law, from the

electrical resistivity of a reference sample measured in four-point geometry. We measure the thicknesses of the Al and PMMA layers by picosecond acoustics<sup>14</sup> using a longitudinal speed of sound of 6.42 nm ps<sup>-1</sup> (Al) and 3.32 nm ps<sup>-1</sup> (PMMA). (The speed of sound of PMMA was determined by picosecond acoustics in a separate experiment on PMMA with known thickness.) The thickness of the NW-composite,  $h=400\pm 20$  nm, was determined from SEM images of the sample structure in cross-section, see Fig. 2b. Since  $\Lambda_C$  is relatively low ( $\Lambda_C/h \ll G$ , where  $G$  is the thermal conductance of the Al/composite interface), our measurements are not sensitive to the value of  $G$ . We thus fix  $G=100$  MW m<sup>-2</sup> K<sup>-1</sup> in the calculations and derive  $\Lambda_C$  by fitting the calculations to the measurements.

In TDTR, at 100 ps delay time, the in-phase signal  $V_{in}$  is mainly controlled by the heat capacity and thickness of the Al film and is only weakly dependent on the thermal properties of the material/sample we are measuring.<sup>22</sup> The out-of-phase signal  $V_{out}$ , on the other hand, is predominantly determined by the out-of-phase response of the surface temperature under periodic heating at the modulation frequency  $f$ ; <sup>22</sup> higher frequency components constitute only less than 10% of the out-of-phase signal  $V_{out}$ .

Under periodic heating at the surface as in the case of TDTR measurements, the distance the heat diffuses into the sample depends on the frequency  $f$  of the heat source; the thermal penetration depth,  $d = \sqrt{\Lambda_C / \pi C_C f}$ , is defined as the distance from the surface at which the amplitude of the temperature oscillation is reduced by a factor  $1/e$ . By varying the modulation frequency  $f$  of the pump beam in the range of 10 MHz to 0.6 MHz, we probe different regions (70-400 nm) of the NW-composite.

We measured the  $\Lambda$  of the NW-composite and the PMMA (a spot in close vicinity of the NW-composite where no NWs were present) using different modulation frequencies  $f$ , and plot the measured  $\Lambda$  as a function of penetration depth  $d$  in Fig. 3. For the PMMA, the thermal conductivity  $\Lambda_{PMMA} \approx 0.2 \pm 0.03$  W m<sup>-1</sup> K<sup>-1</sup> is independent of  $f$  and  $d$ . This value of  $\Lambda_{PMMA}$  is in good agreement with prior measurements using the  $3\omega$  method,  $\Lambda_{PMMA} = 0.19-0.21$  W m<sup>-1</sup> K<sup>-1</sup>.<sup>25</sup> For the NW-composite, however, the measured  $\Lambda_C$  increases with increasing  $d$  for  $1 < f < 10$  MHz ( $70 < d < 300$  nm) and remains constant for measurements with  $f < 1$  MHz ( $d > 300$  nm), see Fig 3.

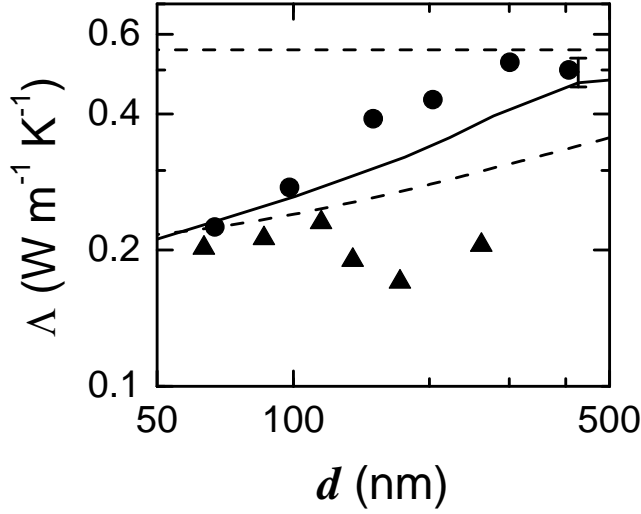


**Figure 3.** Thermal conductivity of a 400 nm-thick NW-composite layer (circles) and a 370 nm-thick PMMA film (triangles) as a function of penetration depth  $d$ , compared to the thermal conductivity derived from FEM simulations (solid line). The dashed lines are limits according to effective medium theory (top) and two-temperature model (bottom) using Eq. (1) and (2) respectively. The error bar is the limits of the thermal conductivity derived from FEM simulations for  $f=0.5$  MHz assuming  $10 \leq G_{Al/NW} \leq 100$  MW m<sup>-2</sup> K<sup>-1</sup> and  $30 \leq G_{PMMA/NW} \leq 300$  MW m<sup>-2</sup> K<sup>-1</sup>. In the FEM simulations and limit calculations, we assume  $G_{Al/NW}=10$  MW m<sup>-2</sup> K<sup>-1</sup>,  $G_{PMMA/NW}=30$  MW m<sup>-2</sup> K<sup>-1</sup>,  $\Lambda_{NW}=6$  W m<sup>-1</sup> K<sup>-1</sup>,  $\Lambda_{PMMA}=0.2$  W m<sup>-1</sup> K<sup>-1</sup>,  $x=0.061$  and  $h=400$  nm. The discrepancy between the FEM simulations for  $f=0.5$  MHz and the effective medium theory limit is about 5-18%.

We propose that the observed dependence of  $\Lambda_C$  on  $f$  is due to a transition between two limiting cases of heat flow in the NW-composite. The heat flow in the NW-composite is complex because the NW-composite consists of channels with higher thermal conductivity (i.e., NWs) embedded in a material with lower thermal conductivity (i.e., PMMA). In addition, heat flow through the higher thermal conductivity channel and heat exchange between the channels are substantially impeded by the interfaces (e.g., Al/NW and PMMA/NW interfaces), and consequently the  $\Lambda_C$  measured by TDTR could also depend on the thermal conductance of the interfaces. Depending on the thermal conductance of the PMMA/NW interfaces,  $G_{PMMA/NW}$ , we propose two fundamental limits of  $\Lambda_C$ , namely the effective medium limit and the two-temperature limit.

In the limit of effective medium theory, we ignore the thermal resistance at the PMMA/NW interfaces ( $G_{PMMA/NW} \rightarrow \infty$ ). We further neglect the thermal conductance of Al/NW ( $G_{Al/NW}$ ) and Al/PMMA ( $G_{Al/PMMA}$ ) interfaces (which are assumed to be  $>30 \text{ MW m}^{-2} \text{ K}^{-1}$ ), as the thermal resistance due to these interfaces (equivalent to  $<20 \text{ nm}$  of NW-composite) is small compared to thermal resistance of the full thickness of the NW-composite. With these assumptions, we treat the NW-composite as a homogenous material and  $\Lambda_C$  is then given by

$$\Lambda_C = x\Lambda_{NW} + (1-x)\Lambda_{PMMA} \quad (1)$$

where  $x$  is the areal packing density of the NW-array and  $\Lambda_{NW}$  is the thermal conductivity of the NWs. We assume that  $\Lambda_C$  measurements at low  $f$  approach the effective medium theory and thus estimate  $\Lambda_{NW} \approx 5.3 \text{ W m}^{-1} \text{ K}^{-1}$ . Simulations by finite element method (FEM), see below, indicate that, depending on the assumed thermal conductance of the interfaces, the thermal conductivity of NW-composite could deviate from calculations of Eq. (1) by  $\sim 18\%$ . Using this value of uncertainty for  $\Lambda_C$ , and assuming that the packing density  $x=0.061$  has a fractional uncertainty of  $15\%$  and  $\Lambda_{PMMA}$  a fractional uncertainty of  $10\%$ , the total propagated uncertainty of the thermal conductivity of the NWs derived using this method is  $\approx 32\%$ .

In the two-temperature limit, we assume that the NWs are thermally insulated from the PMMA and  $G_{PMMA/NW}=0$ . Under such condition, heat flows down the NW-composite through two separate channels (i.e., PMMA-channel and NW-channel). Within the penetration depth distance  $d$ , the thermal resistance of the PMMA-channel equals  $d/\Lambda_{PMMA}$ ; while the thermal resistance of the NW-channel is the sum of the thermal resistance due to the Al/NW interfaces ( $1/G_{Al/NW}$ ) and the thermal resistance of the NW ( $d/\Lambda_{NW}$ ). Assuming that the thermal resistance of the two channels adds in parallel,  $\Lambda_C$  is then given by

$$\Lambda_C = x\left(\Lambda_{NW}^{-1} + G_{Al/NW}^{-1}d^{-1}\right)^{-1} + (1-x)\Lambda_{PMMA} \quad (2)$$

At high  $f$  ( $d \ll \Lambda_{NW}/G_{Al/NW}$ ), the thermal resistance of the NW-channel is dominated by the Al/NW interfaces. We assume that  $\Lambda_C$  measured at high  $f$  approaches  $\Lambda_C$  given by Eq. (2), and adjust the value of  $G_{Al/NW}$  to fit the calculations of Eq. (2) to our measurements at high  $f$ , see Fig. 3. This yields

$G_{Al/NW}=10 \text{ MW m}^{-2} \text{ K}^{-1}$ . This value of  $G_{Al/NW}$  is unreasonably low; the lowest interfacial thermal conductance observed at room temperature for Bi/H-terminated diamond<sup>26</sup> is  $\approx 8 \text{ MW m}^{-2} \text{ K}^{-1}$ , and we hence expect higher  $G_{Al/NW}$  for Al and InAs with more similar speed of sounds and Debye temperatures. The reason of this unrealistic value of  $G_{Al/NW}$  is unknown to the authors. We stress however, that our method of deriving the thermal conductivity of NWs from TDTR measurements at low  $f$  does not rely on the knowledge of the accurate value of  $G_{Al/NW}$ . FEM simulations discussed below show that  $\Lambda_C$  approaches the effective medium limit at low  $f$  regardless of assumed  $G_{Al/NW}$ .

We verify our hypothesis that  $\Lambda_C$  approaches the effective medium theory at low  $f$  with simulations of a finite-element method (FEM) model.<sup>27</sup> In the FEM model, we construct an infinite array of InAs NWs 400 nm long and 52 nm in diameter, embedded in PMMA on an InAs substrate, where we assume that  $x=0.061$ ,  $\Lambda_{NW}=6 \text{ W m}^{-1} \text{ K}^{-1}$ ,  $\Lambda_{PMMA}=0.2 \text{ W m}^{-1} \text{ K}^{-1}$  and  $\Lambda_{InAs}=27 \text{ W m}^{-1} \text{ K}^{-1}$ . We apply periodic heating of frequency  $f$  at the surface and simulate the temperature oscillations at the surface using the FEM model.

We derive  $\Lambda_C$  of the NW-composite from the FEM model by comparing the FEM simulations to analytical calculations<sup>28</sup> of 1-D heat transport across a tri-layered structure consisting of a NW-composite layer on an InAs substrate coated with a 90 nm Al film, similar to our FEM model. In the analytical calculations, we assume that the NW-composite layer is homogeneous, and adjust  $\Lambda_C$  of the layer to fit the calculations to the simulated out-of-phase temperature rise at the surface. We fit the out-of-phase temperature rise, instead of the amplitude of the temperature oscillations, to mimic the TDTR measurements. We validate our approach by deriving  $\Lambda_{PMMA}$  from FEM simulations on a similar structure with the NW-composite layer being substituted by a homogeneous PMMA layer;  $\Lambda_{PMMA}$  derived from these FEM simulations matches the value for  $\Lambda_{PMMA}$  we set in the FEM program to within 2%.

We plot  $\Lambda_C$  derived from the FEM simulations assuming  $G_{Al/NW}=10 \text{ MW m}^{-2} \text{ K}^{-1}$  and  $G_{PMMA/NW}=100 \text{ MW m}^{-2} \text{ K}^{-1}$  as a solid line in Fig. 3. We find that  $\Lambda_C$  derived from the FEM simulations transitions from the two-temperature limit at high frequencies ( $f \approx 10 \text{ MHz}$ ;  $d \approx 70 \text{ nm}$ ) to the effective medium theory at

low frequencies ( $f < 1$  MHz;  $d > 300$  nm), see Fig. 3. As we are not able to independently measure  $G_{Al/NW}$  and  $G_{PMMA/NW}$ , we vary  $G_{Al/NW}$  from 10 to 100 MW m<sup>-2</sup> K<sup>-1</sup> and  $G_{PMMA/NW}$  from 30 to 300 MW m<sup>-2</sup> K<sup>-1</sup> in the FEM simulations. We find that  $\Lambda_C$  at  $f=0.5$  MHz derived from FEM simulations are only weakly dependent on the values of  $G_{Al/NW}$  and  $G_{PMMA/NW}$ ;  $\Lambda_C=0.46\text{--}0.53$  W m<sup>-1</sup> K<sup>-1</sup> for any combination of  $G_{Al/NW}$  and  $G_{PMMA/NW}$  used, see Fig. 3, close to the effective medium theory limit for  $x=0.061$  of  $\Lambda_C=0.55$  W m<sup>-1</sup> K<sup>-1</sup>.

A possible explanation for the transition of  $\Lambda_C$  between two limits is that the temperature difference between the NWs and the PMMA is eliminated after a characteristic distance, the thermal healing length,  $l_h$ . At low heating frequencies  $f \ll G_{eff}/(\pi r C_{NW})$ , where  $G_{eff}$  is the effective thermal conductance of NW walls given by Eq. (4), and  $r$  and  $C_{NW}$  are the radius and the volumetric heat capacity of NWs, respectively, the healing length is approximately<sup>29</sup>

$$l_h = \sqrt{\frac{r\Lambda_{NW}}{2G_{eff}}} \quad (3)$$

For NWs embedded in PMMA, heat flow through the side walls of the NWs is predominantly controlled by the thermal conductance of the PMMA matrix, rather than the thermal conductance of the PMMA/NW interfaces. Thus, we approximate  $G_{eff}$  from the analytical solution of heat flow in cylindrical coordinates and obtain

$$G_{eff} = \frac{\Lambda_{PMMA}}{r \ln(R/r)} \quad (4)$$

where  $2R$  is the distance between adjacent NWs. By substituting Eq. (4) into Eq. (3), we derive

$$l_h = r \sqrt{\left(\frac{\Lambda_{NW}}{\Lambda_{PMMA}}\right) \left(\frac{\ln(R/r)}{2}\right)} \quad (5)$$

Note that  $l_h$  depends on the radius of NWs and the ratio of thermal conductivity of NWs and PMMA, but not on the thermal conductance of interfaces.

For the case of our experiment,  $\Lambda_{NW} \approx 6$  W m<sup>-1</sup> K<sup>-1</sup>,  $\Lambda_{PMMA} = 0.2$  W m<sup>-1</sup> K<sup>-1</sup>,  $r = 26$  nm,  $R = 100$  nm; hence  $G_{eff} \approx 5.7$  MW m<sup>-2</sup> K<sup>-1</sup> and  $l_h \approx 120$  nm. Thus, for  $d < 120$  nm, the NWs and PMMA are essentially

decoupled and  $\Lambda_C$  of the NW-composite approaches the two-temperature limit given by Eq. (2), see Fig. 3. However, as  $f$  decreases and  $d$  increases, thermal equilibrium is reached across the PMMA/NW interfaces for a larger volume of the NW-composites. As a result,  $\Lambda_C$  increases as more heat bypasses the resistive Al/NW interfaces and flows through the more conductive NWs. For the case of  $f < 1$  MHz and  $d \gg l_h$ , NWs and PMMA are strongly coupled, and  $\Lambda_C$  approaches the prediction of the effective medium theory given by Eq. (1).

$\Lambda_{NW} = 5.3 \text{ W m}^{-1} \text{ K}^{-1}$  of the InAs nanowires derived using this approach agrees well with prior measurement on a suspended InAs nanobeam<sup>6</sup> of  $4.1 \text{ W m}^{-1} \text{ K}^{-1}$ . The thermal conductivity of the nanobeam was measured using a microfabricated device in vacuum. The rectangular InAs nanobeam had similar thickness (40 nm thick, 150 nm wide), but was exposed to reactive ion etching and wet etching prior to the measurements, which could explain the lower value of the measured thermal conductivity.

Our measurement also compares well with the prediction of a Callaway-type model<sup>22,30</sup> assuming an additional boundary scattering term of  $\tau^{-1} = D/v$ , where  $D$  is the diameter of the NWs and  $v$  is the speed of sound;  $\Lambda_{NW} = 7 \text{ W m}^{-1} \text{ K}^{-1}$  according to the model. In the model, we include acoustic phonons with velocity close to the speeds of sound using cutoff frequencies<sup>30</sup> from the phonon dispersion. We derive the strength of anharmonic scattering<sup>22</sup> by fitting the calculations to the thermal conductivity of bulk InAs, and take into account heat conduction due to the diffusion of the high frequency acoustic and optical phonons.<sup>31</sup> The calculated  $\Lambda_{NW}$  using this Callaway-type model is close to prior calculations by Mingo<sup>32</sup> of  $\Lambda_{NW} \approx 3.5\text{--}7 \text{ W m}^{-1} \text{ K}^{-1}$  for InAs NWs of 50 nm diameter. The wide range in Mingo's calculations is due to different assumptions of degree of specularly for boundary scattering.

We have demonstrated a technique to measure the thermal conductivity of NWs in NW-arrays and NW-composites. We found that the thermal conductivity  $\Lambda_C$  of NW-composite measured by TDTR is independent of modulation frequency  $f$  used in the measurements when  $f$  is sufficiently low. Our FEM simulations indicate that this  $\Lambda_C$  measured at low  $f$  approaches the thermal conductivity predicted by

effective medium theory. Using this approach, we derived the thermal conductivity of 52 nm diameter InAs NWs embedded in PMMA to be  $5.3 \text{ W m}^{-1} \text{ K}^{-1}$ , approximately five times lower than the value for bulk InAs. This value of thermal conductivity is in good agreement with prior measurements and calculations on isolated NWs, supporting the validity of our approach for the composite heat conductance. This technique could be useful to investigate the heat transport in NW-arrays embedded in a matrix material, a more likely structure for future NW-based devices.

This work was supported by Office of Naval Research (ONR) grants no N-00014-05-1-0902 and 0903, ONR grant no N00014-07-1-0190, U.S. Department of Energy grant no DEFG02-91ER45439, the ONR/ONAMI Nanometrology Initiative, the Royal Physiographic Society in Lund, the Swedish Foundation for Strategic Research (SSF), the Swedish Research Council (VR) and Knut and Alice Wallenberg Foundation.

- (1) Cahill, D. G.; Ford, W. K.; Goodson, K. E.; Mahan, G. D.; Majumdar, A.; Maris, H. J.; Merlin, R.; Phillpot, S. R. *J. Appl. Phys.* **2003**, *93*, 793
- (2) Zou, J.; Balandin, A. *J. Appl. Phys.* **2001**, *89*, 2932
- (3) Walkauskas, S. G.; Broido, D. A.; Kempa, K.; Reinecke, T. L. *J. Appl. Phys.* **1999**, *85*, 2579
- (4) Tighe, T. S.; Worlock, J. M.; Roukes, M. L. *Appl. Phys. Lett.* **1997**, *70*, 2687
- (5) Shi, L.; Li, D.; Yu, C.; Jang, W.; Kim, D.; Yao, Z.; Kim, P.; Majumdar, A. *J. Heat Transfer* **2003**, *125*, 881
- (6) Mavrokefalos, A.; Pettes, M. T.; Saha, S.; Zhou, F.; Shi, L. *25<sup>th</sup> International Conference on Thermoelectrics* **2006**, 234
- (7) Guthy, C.; Nam, C. -Y.; Fischer, J. E. *J. Appl. Phys.* **2008**, *103*, 064319
- (8) Hochbaum, A. I.; Chen, R.; Delgado, R. D.; Liang, W.; Garnett, E. C.; Najarian, M.; Majumdar, A.; Yang, P. *Nature* **2008**, *451*, 163

- (9) Yang, R.; Chen, G.; Dresselhaus, M. S. *Phys. Rev. B* **2005**, *72*, 125418
- (10) Prasher, R. *J. Appl. Phys.* **2006**, *100*, 034307
- (11) Bryllert, T.; Wernersson, L. –E.; Fröberg, L. E.; Samuelson, L. *IEEE Electron Dev. Lett.* **2006**, *27*, 323
- (12) Pokatilov, E. P.; Nika, D. L.; Balandin, A. A. *Superlattices and Microstructures* **2005**, *38*, 168
- (13) Yang, R.; Chen, G.; Dresselhaus, M. S. *Nano Lett.* **2005**, *5*, 1111
- (14) Capinski, W. S.; Maris, H. J.; Ruf, T.; Cardona, M.; Ploog, K.; Katzer, D. S. *Phys. Rev. B* **1999**, *59*, 8105
- (15) Costescu, R. M.; Wall, M. A.; Cahill, D. G. *Phys. Rev. B* **2003**, *67*, 054302
- (16) Jensen, L. E.; Björk, M. T.; Jeppesen, S.; Persson, A. I.; Ohlsson, B. J.; Samuelson, L. *Nano Lett.* **2004**, *4*, 1961
- (17) Persson, A. I.; Fröberg, L. E.; Samuelson, L.; Linke, H. *Nanotechnology* **2009**, *20*, 225304
- (18) Young, D. A.; Thomsen, C.; Grahn, H. T.; Maris, H. J.; Tauc, J. in *Phonon Scattering in Condensed Matter*; Anderson, A. C.; Wolfe, J. P., Eds; Springer: Berlin, **1986**, 49-51
- (19) Paddock, C. A.; Eesley, G. L. *J. Appl. Phys.* **1986**, *60*, 285
- (20) Kang, K.; Koh, Y. K.; Chiritescu, C.; Zheng, X.; Cahill, D. G. *Rev. Sci. Instrum.* **2008**, *79*, 114901
- (21) Cahill, D. G. *Rev. Sci. Instrum.* **2004**, *75*, 5119
- (22) Koh, Y. K.; Cahill, D. G. *Phys. Rev. B* **2007**, *76*, 075207
- (23) *Thermophysical Properties of Matter*, Touloukian Y. S.; Buyco E. H., Eds; Plenum: New York, **1970**

- (24) Bu, H. S.; Aycock, W.; Wunderlich, B. *Polymer* **1987**, 28, 1165
- (25) Putnam, S. A.; Cahill, D. G.; Ash, B. J.; Schadler, L. S. *J. Appl. Phys.* **2003**, 94, 6785
- (26) Lyeo, H. -K.; Cahill, D. G. *Phys. Rev. B* **2006**, 73, 144301
- (27) The FEM simulations were performed with a commercial FEM package, ABAQUS.
- (28) Feldman, A. *High Temp. – High Press.* **1999**, 31, 293
- (29) Carslaw, H. S.; Jaeger, J. C. *Conduction of Heat in Solids*, Oxford University Press, **1959**, p. 137.
- (30) Morelli, D. T.; Heremans, J. P.; Slack, G. A. *Phys. Rev. B* **2002**, 66, 195304
- (31) Koh, Y. K.; Cao, Y.; Cahill, D. G.; Jena, D. *Adv. Funct. Mater.* **2009**, 19, 610
- (31) Mingo, N. *Appl. Phys. Lett.* **2004**, 84, 2652, and erratum: *Appl. Phys. Lett.* **2006**, 88, 149902